Available online at www.sciencedirect.com
SCIENCE DIRECT®
ELSEVIER
Nuclear Instruments and Methods in Physics Research B 225 (2004) 241–255
NIM B
Beam Interactions with Materials & Atoms
www.elsevier.com/locate/nimb

Structural and sputtering effects of medium energy ion bombardment of silicon

M.C. Moore [a], N. Kalyanasundaram [a,*], J.B. Freund [b], H.T. Johnson [a,*,1]

[a] *Department of Mechanical and Industrial Engineering, University of Illinois at Urbana-Champaign, 1206 W. Green St., Urbana, IL 61801, USA*

[b] *Department of Theoretical and Applied Mechanics, University of Illinois at Urbana-Champaign, Urbana, IL 61801, USA*

Received 23 February 2004; received in revised form 2 April 2004

Abstract

Molecular dynamics simulation is used to study argon ion bombardment of an initially perfect silicon crystal up to its damaged state at a total fluence of 4×10^{14} impacts/cm^2. Lower and higher energy processes are considered: one process with ions at 500 eV and another process with ions at 700 eV, which are like those used in a particular microelectromechanical systems (MEMS) fabrication technique. These energies are intermediate relative to most previous silicon ion bombardment studies, higher than those typically used in ion-assisted deposition and lower than in typical ion implantation. In all, up to 118 impacts are simulated in a 5.43 by 5.43 nm periodically replicated cell of a target (0 0 1) surface of silicon. After an impact, the material is cooled slowly to 77 K by a process that models thermal conduction in to the bulk target material. It is assumed that defects are immobile at this temperature and that no further structural relaxation occurs before the next impact. Multiple simulations of more than 100 ion impacts are conducted for both ion energies and averaged to converge statistical descriptions of structural evolution and sputtering. Surface roughening is observed with increase in ion fluence. Damage throughout the sample is studied using a planar radial distribution function. Using a crystallinity measure based on this function, it is found that the damage region extends 2.2 nm into the material for 500 eV ions and 3.0 nm for 700 eV ions after 80 impacts. The damaged region is separated from deeper, undamaged crystal by a nearly flat interface. Sputter yields are in reasonable agreement with experimental data, reaching nearly steady rates of 0.5 and 0.7 sputtered atoms per incident argon atom for the 500 and 700 eV cases, respectively. For the number of ions considered, implanted argons do not significantly affect Si sputtering.

PACS: 79.20.R; 61.43.B; 61.43.D; 61.20.J; 81.05.G
Keywords: Molecular dynamics calculations; Ion sputtering; Structure; Amorphization

1. Introduction and background

Chemically neutral ion beam machining of silicon MEMS devices has recently been demonstrated as a useful and efficient process to tailor the residual stress distribution in free-standing

* Corresponding authors. Tel.: +1-217-244-5977; fax: +1-217-244-6534 (N. Kalyanasundaram), tel.: +1-217-265-5468 (H.T. Johnson).
E-mail addresses: klynsndr@uiuc.edu (N. Kalyanasundaram), htj@uiuc.edu (H.T. Johnson).
[1] 362 B, Mechanical Engineering Building, 1206, W. Green St., Urbana, IL 61801, USA.

0168-583X/$ - see front matter © 2004 Elsevier B.V. All rights reserved.
doi:10.1016/j.nimb.2004.04.175

thin-film structures [1]. The ion kinetic energies used in this procedure (~500 eV) are higher than those used in most mild surface modification or deposition processes but significantly lower than those typically used in ion implantation. Its purpose is to damage the silicon in a way that creates a residual stress that alters the mean curvature of the film. However, the effects of the process on near-surface atomic structure and sputtering of silicon atoms are not understood in detail. The process is intended to tailor the properties of a structure used for optical purposes, so the near-surface structure and crystalline quality is particularly important to understand. Material removal is also an important feature of the process, so it is critical to understand sputtering behavior for the process. In this work molecular dynamics (MD) simulation is used to study these issues.

Several different methods for simulating ion bombardment are reported in the literature, not all of which are suitable for the study of multi-impact structure and sputtering behavior. If the objective is only to study the annealed damage pattern of a single impact, then the dynamics of the collision itself can be omitted from the simulation [2,3]. In such an approach, approximations to the damage of interest are inserted into the lattice and equilibrated and then often annealed using MD. Another approach is the "knock-on" atom method [4]. Here, too, the ion itself is not directly simulated; instead a surface atom is simply assigned a velocity corresponding to a direct impact with the incident ion. This method is used to track the dynamics of the collision cascade. For 5 keV energies, Díaz de la Rubia and Gilmer [4] demonstrate that defect production and structural transformations can be investigated using knock-on atoms, but it is not clear how well such an approach would represent the details of multiple ion impacts. In this study a more direct approach is pursued, whereby an ion is explicitly included in the simulation with an appropriate potential governing its interactions with silicon as in [5].

Ion bombardment or ion processing is used in several applications including plasma-vapor deposition [6], dopant insertion [7] and amorphization or crystallization [8]. Most applications use either low ion energies, with kinetic energy of 200 eV or less, or high energies between 1 and 100 keV, though some reach as high as 1 MeV, and these energies have received the greatest attention in the literature. Relatively little work has been done in the 500 eV to 1 keV energy range. It is not well understood, for example, how near-surface damage evolves as a function of fluence. It is also unclear how sputter yields in this energy range change as the initially undamaged surface gradually evolves into a fully rough surface during ion bombardment.

Work on low energy ion irradiation generally focuses on sputtering rates [6,9–11], surface damage and defects [12,13], or deposition of ions on the surface [6,10,13,14]. In several studies [6,9,10], passivated silicon is bombarded with 25–200 eV ions and computed sputtering rates are in reasonable agreement with experiments. It is typically found that higher argon fluence increases the Si sputter yield and that sputter yield is insensitive to temperature. Silicon sputtering is analyzed by Rubio et al. [15] for 1 keV ion energy ranges, and it is found that sputter yield increases with argon content, though in this work ions are inserted directly rather than embedded dynamically. They conclude that sputtering is more likely on surfaces above locally high argon concentrations, which is also examined in the present work at fluence levels of interest here.

Other studies at higher energies examine damage and recrystallization. Díaz de la Rubia and Gilmer [4] and Caturla et al. [16] study the single impact damage cascade for 1–15 keV bombardment of silicon and report that this region has a structure that most closely resembles quenched liquid silicon. The amorphous region generated by bombardment can be recrystallized by short annealing sessions at high temperatures leaving only point defects [16]. Explicit simulations are computationally costly for energies greater than 1 MeV, but the effects of ion bombardment at these high energies have been studied by inserting the damage [2,17] or by only simulating secondary cascades [18,19].

The effect of kinetic relaxation on statistical structure and sputtering trends is a critical issue but is difficult to directly resolve using molecular dynamics. Molecular dynamics simulations are

typically limited to overall simulation times on the order of nanoseconds due to computational expense. However, for a small ($\sim$nm^2) element of surface, whose atoms' trajectories can be tracked in a simulation, there is well over 1 μs between impacts in typical applications. Between impacts, annealing may occur over time spans that are too long to be explicitly represented in MD simulations. There is experimental evidence that vacancies and interstitials are activated at relatively low temperatures (150 K), so annealing should be expected [20,21], though most of it will surely occur in the first few picoseconds following the impact, when the material is still locally hot from the ion's energy. In their study of sputtering behavior due to multiple off-normal incidence impacts, Haddeman and Thijsse [11] neglect any long-time structural relaxation between impacts. In the present work this issue is handled by explicitly simulating cooling to a low ambient temperature at which defects are thought to be mobile. The technique is described along with the basic simulation methodology in the following section, which is followed in turn by a discussion of simulation results.

2. Simulation methodology

Stillinger–Weber potential [22] is used to model silicon–silicon interactions and Molière potential [23,24] is used to model argon–silicon and argon–argon interactions. The Molière potential is a common choice in ion impact studies [5,6,10,11,25]. Its functional form is

$$\Phi = Z_i Z_j \frac{q^2}{r}\left\{0.35\exp\left(-0.3\frac{r}{a}\right)+0.55\exp\left(-1.2\frac{r}{a}\right)+0.10\exp\left(-6.0\frac{r}{a}\right)\right\}, \quad (1)$$

where Z_i and Z_j are atomic numbers of the ith and jth atoms, q is the electron charge, r is the distance between atoms and a is the Firsov screening length [5],

$$a = 0.885 a_0 (Z_i^{1/2} + Z_j^{1/2})^{-2/3}, \quad (2)$$

in which a_0 is the Bohr radius. The attractive part of the argon–argon and argon–silicon interactions can be assumed to be small and may be neglected because the primary purpose of argon atoms is to transfer energy and momentum, but not to participate in chemical bonding [25]. Hence a purely repulsive Molière potential is used. The velocity-Verlet algorithm is used to integrate the equations of motion to track the atomic trajectories. The numerical time step is $\Delta t = 0.25$ fs, except during the initial stages of the ion impact when Δt is reduced to 0.1 fs in order to resolve the initial collisions. It was verified directly that this is sufficient by comparing results to simulations with even shorter time steps.

To control temperature, at each time step the velocities are rescaled according to [26]

$$V = \lambda V,$$
$$\lambda = \left[1 + \frac{\Delta t}{\tau}\left(\frac{T_0}{T} - 1\right)\right]^{1/2}, \quad (3)$$

where V is the velocity, λ is the rescaling factor, Δt is the numerical time step size, τ parameterizes the strength of the thermostat, T_0 is the target temperature and T is the current temperature. Because this thermostat does not correspond to any physical process, it is only used for certain periods and on certain atoms during the course of the simulation. Where and when this thermostat is applied is described in the following discussion of the simulation procedure.

For all simulation presented in this paper, the sample material is modeled by a periodically repeated 5.43 nm × 5.43 nm × 5.43 nm cube consisting of 8000 silicon atoms as shown schematically in Fig. 1. The transverse box size is selected so that there are no perceived effects of the x and y periodic boundary conditions. The (0 0 1) surface is exposed to vacuum on the top and 200 atoms in the bottom plane are held fixed to maintain the position of the sample. During an impact, the thermostat is applied only to the bottom two silicon crystallographic unit cells ($\sim$1 nm) to model cooling by thermal conduction into the sample. The extent of the crystal in z is set so that these thermostated planes are far from the impact area and thus do not directly affect the damaged regions. The x and y position of each argon atom is

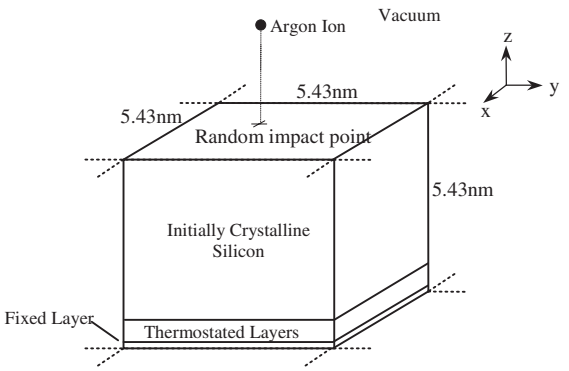

Fig. 1. Simulation schematic.

randomly selected before its velocity is set for normal incidence impact.

A representative ion impact event is described here using the mean temperature history plotted in Fig. 2 to mark significant events during its impact. The simulation begins with the thermostat applied to all atoms to equilibrate the target material to 77 K. When this temperature is reached (**a** in the figure), the first argon ion is assigned a velocity normal to the surface of the silicon and is included in the temperature average. This causes the spike in temperature seen at point **b** in the figure. Once the argon hits the surface, the mean temperature decreases (**c** in the figure) and the thermostat is activated at the bottom of the domain. The sample then slowly cools back to 77 K. This temperature is chosen because it is experimentally realizable and because it is reported that for temperatures less than 150 K defects are effectively immobile [20,21]. Partyka et al. [21] show that thermally activated motion of interstitials can happen at temperatures as low as ~150 K, with vacancy motion beginning above 175 K. Based on this observation, it is assumed that once the system has cooled to 77 K, thermally activated processes will be limited so no significant changes are expected. Thus, it is assumed here that no further structural changes occur in the greater than 1 μs between impacts in this 5.43 nm × 5.43 nm section of the sample. When the target temperature of 77 K is reached (**d** in the figure) the system is quenched to 4 K (**e** in the figure) to freeze the damage in the system, allowing for a stress analysis. The entire process is then repeated with the next ion.

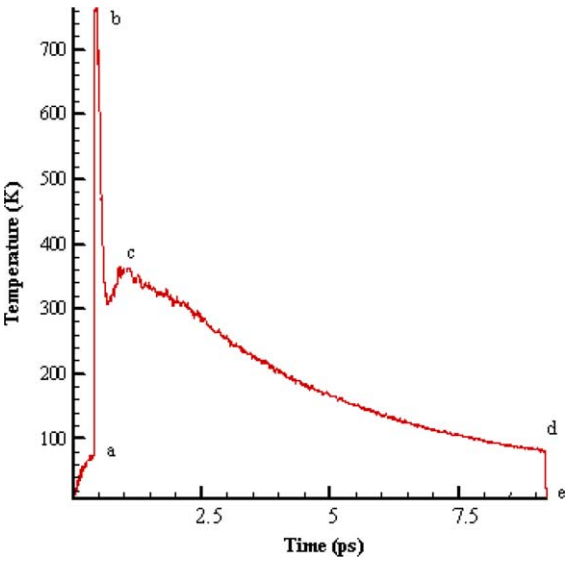

Fig. 2. Temperature profile versus time for one ion impact on the silicon surface.

3. Results and discussion

Two separate sets of simulations are discussed here, one with ion velocities corresponding to 500 eV and the other with incident ions at 700 eV, both at normal incidence. For the 500 and 700 eV energies, 8 and 7 cases are run, respectively, for a total of 15 simulations. These multiple ensembles are used to converge statistics. For each case the initial velocities of the silicon atoms and the positions of the argon are randomly selected. Some of the results reported below represent data that are averaged over these ensembles, while other data, as noted, represent individual cases.

3.1. Structure

3.1.1. Structural evolution through damage and defects

Upon ion bombardment, crystalline defects are introduced into the diamond cubic structure. Though some are immediately annihilated, the defects increase in number with ion fluence, leading to a highly damaged system. The damaged

state may be viewed as a crystalline system containing a complex combination of vacancies and interstitials near the regions of ion impact. The regions nearest the ion impacts only resemble crystals with point defects for the very smallest fluences, however. The defects created near the end of each cascade, where the incident kinetic energy is lowest, better exhibit qualities of simple vacancy–interstitial pairs, but with an occasional extra vacancy or interstitial.

Fig. 3 shows the damage evolution for the 500 eV case as a series of side view [0 1 0] images, where the surface normal to the incident ion direction is [0 0 1]. After two incident ions, defects are found near the surface of the crystal. As the number of implanted ions increases, the damage to the surface becomes more pronounced until after 20 ions the entire original surface has been damaged. As more ions bombard the surface the depth of the damage increases. Point defects are found in the lower portion of the system where the material remains essentially crystalline. Finally after 80 ions, corresponding to a fluence of nearly 3.0×10^{14} ions/cm^2, a well defined damaged region exists in the top 2–3 nm of the sample with a relatively flat interface between it and the crystal below.

The damage evolution process is similar for the 700 eV case. For comparison, Fig. 4 shows the damage after 80 ions for both the 500 and 700 eV cases. The 500 eV case has a more clearly defined interface; the interface between damaged and

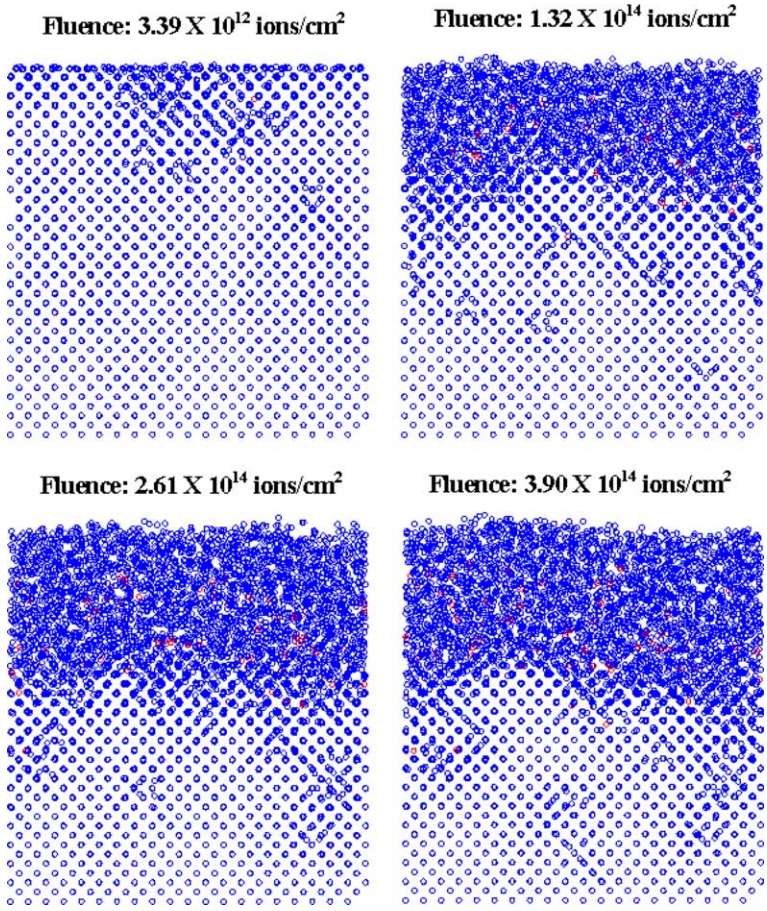

Fig. 3. Damage evolution for argon ion energy of 500 eV. Blue denotes silicon, argon is red.

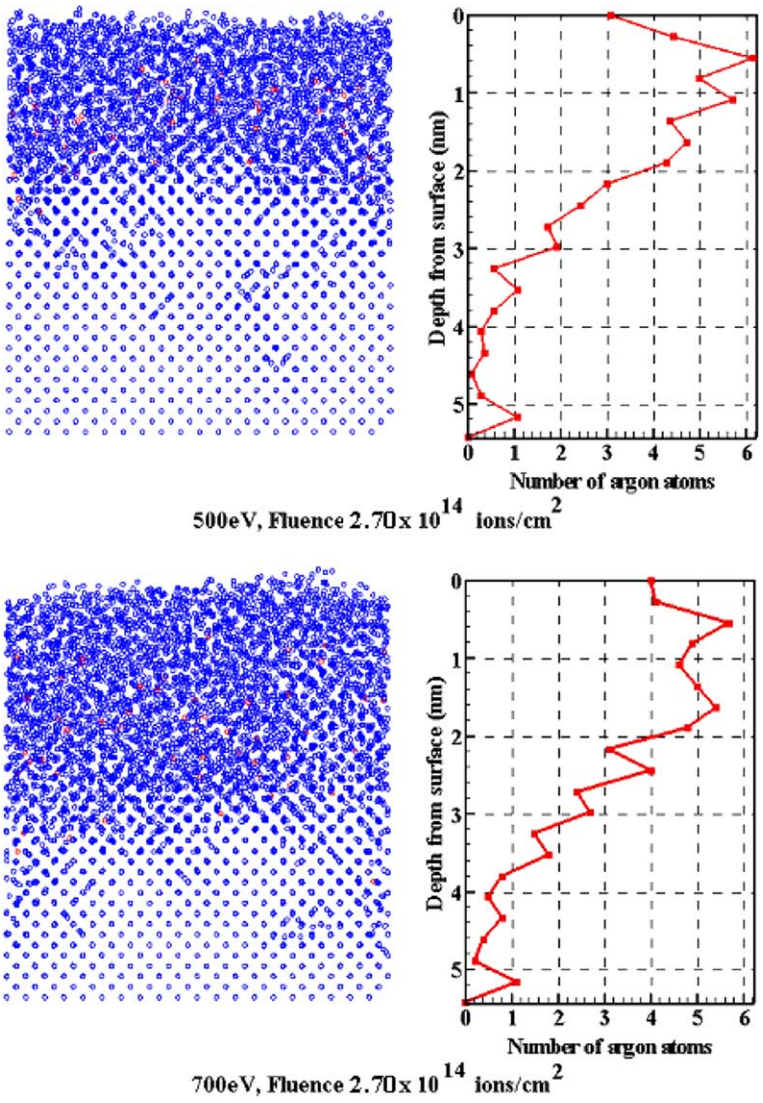

Fig. 4. Comparison of damage after 80 ions for the 500 and 700 eV cases. Blue denotes silicon, argon is red. The number of argon atoms present in a layer of 0.2 nm, averaged over 8 and 5 separate randomized cases for 500 and 700 eV ion energies, respectively, is shown as a function of depth from surface on the right. The distribution of argon atoms peaks at a depth from surface.

crystalline regions of the 700 eV case is more diffuse. The damaged region in the 700 eV case penetrates deeper into the crystal with more defects located in the crystalline region. Structure as a function of depth is discussed in the following section. In both the 500 eV case and the 700 eV case the argon atoms are largely contained in the damaged layer, while some penetrate into the crystalline region. But the maximum argon concentration occurs closer to the surface in the 500 eV case than in the 700 eV case, as shown in Fig. 4. In both cases few argon atoms are present in the top 0.8–1 nm, as argon atoms near the surface escape during the short annealing stage between ion impacts. In both cases the surface of the silicon roughens considerably.

3.1.2. Planar radial distribution function

To quantify the structure and its evolution, a planar radial distribution function is calculated in x–y layers parallel to the free surface. The probability $g(r)$ of finding a pair of atoms a distance r apart, relative to the probability expected for a completely random distribution at the same density, is given by

$$g(r) = \left\langle \frac{A}{N_l} \sum_i \sum_{j \neq i} \delta(\mathbf{r} - \mathbf{r}_{ij}) \right\rangle, \tag{4}$$

where A is the area of the layer, N_l is the number of atoms per layer l and $\mathbf{r}_{ij}$ is the projection to the x–y plane of the vector $\mathbf{r}_i - \mathbf{r}_j$ that joins the atoms with position vectors $\mathbf{r}_i$ and $\mathbf{r}_j$. The angular brackets indicate an average over all atoms in the layer. The planar radial distribution function is calculated using a histogram or binning [27] based on counting the number of atoms j in the kth bin from atom i, so that the distribution function is given by

$$g(r) = \left\langle \frac{A}{N_l} \frac{h_k(r_{ij} : \Delta r)}{2\pi r \Delta r t} \right\rangle, \tag{5}$$

such that

$$(k-1)\Delta r \leqslant |\mathbf{r}_{ij}| < k\Delta r, \tag{6}$$

$$r = (k-1)\Delta r \tag{7}$$

and

$$N_l = \frac{N_v}{t}, \tag{8}$$

where r is the planar distance from atom i to the kth bin (7), Δr is the bin size and N_v is the number of atoms contained in a volume described by layer area A and thickness t in a direction perpendicular to layer area. The function $h_k(r_{ij} : \Delta r)$ is defined as the number of atoms j in the kth bin from atom i. A layer thickness of 0.2 nm was used in calculating $g(r)$.

The planar radial distribution function, $g(r)$, is used to probe the structure at various depths in the material to quantify the damage and its evolution. Fig. 5 shows the planar radial distribution function for the 500 eV ion energy case, averaged over 8 separate randomized cases, for layers corresponding to 1, 2 and 4 nm from the original surface representing relatively damaged and crystalline regions and a layer in between.

The periodic crystalline structure evident in the bottom of Fig. 5 is not as pronounced at depth of 2 nm and is virtually absent at a depth of 1 nm from the free surface. The damaged region has a liquid-like $g(r)$ [27] that indicates an amorphous or non-periodic structure. This is consistent with some previous experimental work, which shows that pure amorphous silicon can be created to a depth of 8 μm by self-bombardment at 17 MeV [28]. More kinetic energy is deposited in the system in that case, but local amorphization may be occurring here at smaller energies.

3.1.3. Degree of crystallinity

The planar radial distribution function determined in the previous section is used to calculate a measure of crystallinity. This analysis is similar to the calculation of a crystallographic static structure factor. In order to define a measure of crystallinity, the Fourier sine transform $F^S(k)$ of $(g(r) - 1)$ is calculated using

$$F^S(k) = \int_0^\infty (g(r) - 1) \sin(2\pi k r)\, \mathrm{d}r, \tag{9}$$

where k is the wave vector.

The degree of crystallinity, χ, is then defined by

$$\chi = A\rho_{2\mathrm{D}} \left| \int_0^{k_{\max}} \frac{1}{k} F^S(k)\, \mathrm{d}k \right|, \tag{10}$$

where $\rho_{2\mathrm{D}}$ is the planar number density, $k_{\max}$ is the wave vector at which $|F^S(k)|$ is maximum and A is a normalization constant which ensures that crystalline material has a value of χ equal to 1. By this definition, a liquid-like radial distribution function has χ close to 0.

Figs. 6 and 7 show evolution of crystallinity as the ion bombardment process progresses for individual 500 and 700 eV cases, respectively. From these figures, it can be seen that material near the surface is essentially amorphous at fluences as low as about 1×10^{14} ions/cm^2 for the both the 500 eV case and the 700 eV case. In the transformation from crystalline to amorphous Si, a plateau region between $\chi = 0.2$ and $\chi = 0.25$ is observed in both cases. The plateau indicates a persistence of structure in the transformation process. While

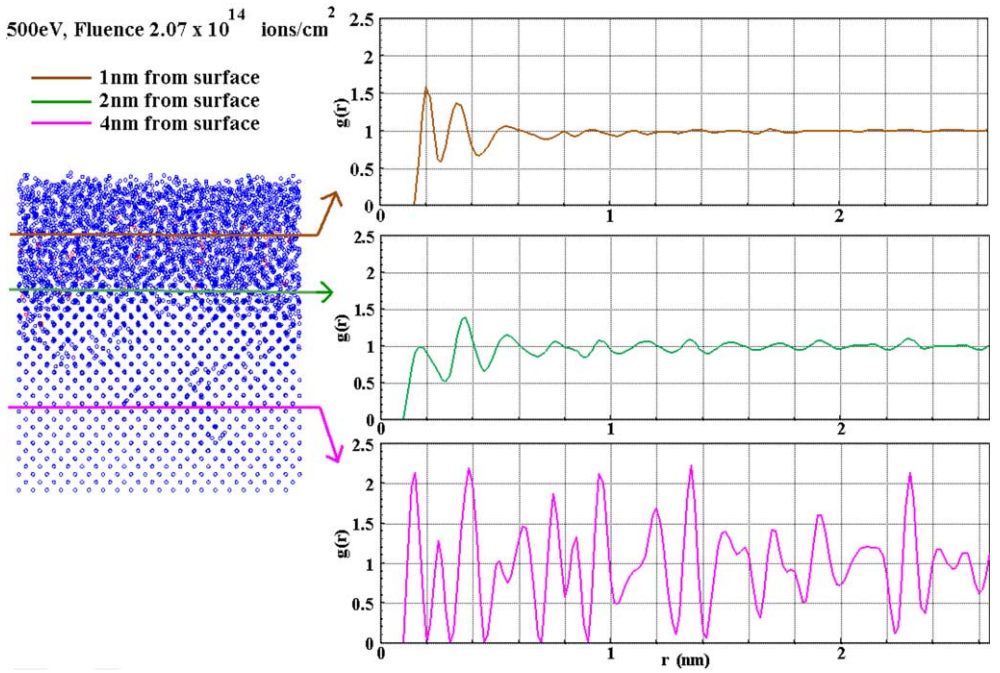

Fig. 5. Planar radial distribution as a function of radial distance after fluence of 2.07×10^{14} ions/cm^2 (61 ions) for the 500 eV case. Data presented here are averaged over 8 separate randomized cases. The layers correspond to planes at depths of 1, 2 and 4 nm, and are indicative of damaged, interface and crystalline regions, respectively.

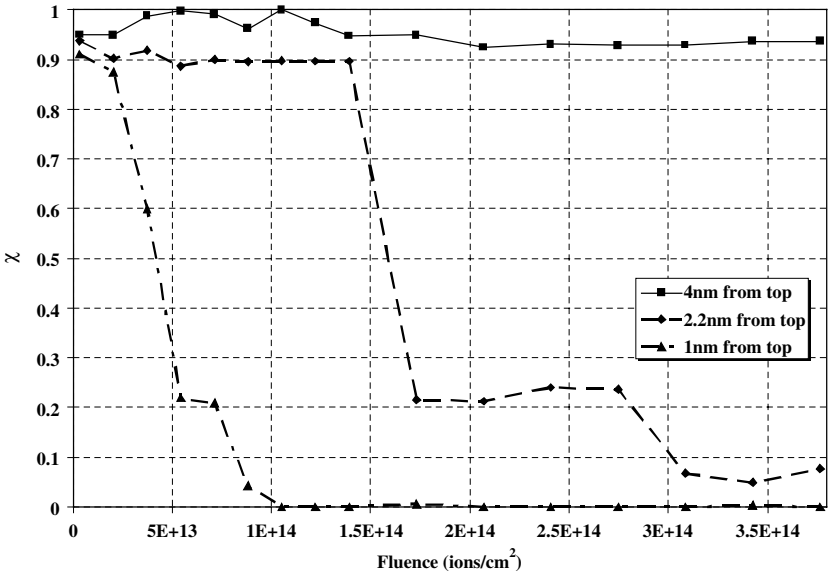

Fig. 6. Plot of crystallinity with respect to argon fluence at three depths from the surface for the 500 eV case.

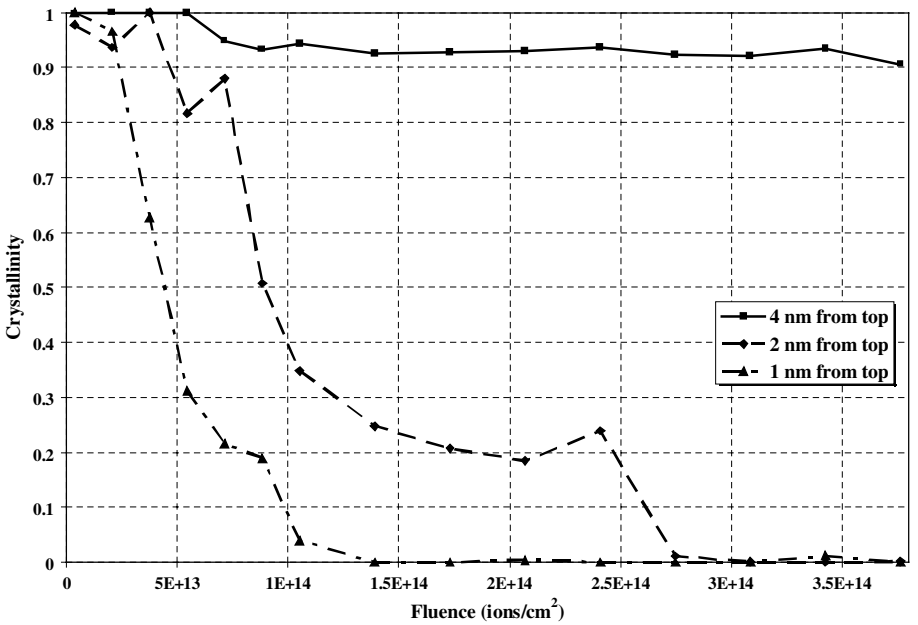

Fig. 7. Plot of crystallinity with respect to argon fluence at three depths from the surface for the 700 eV case.

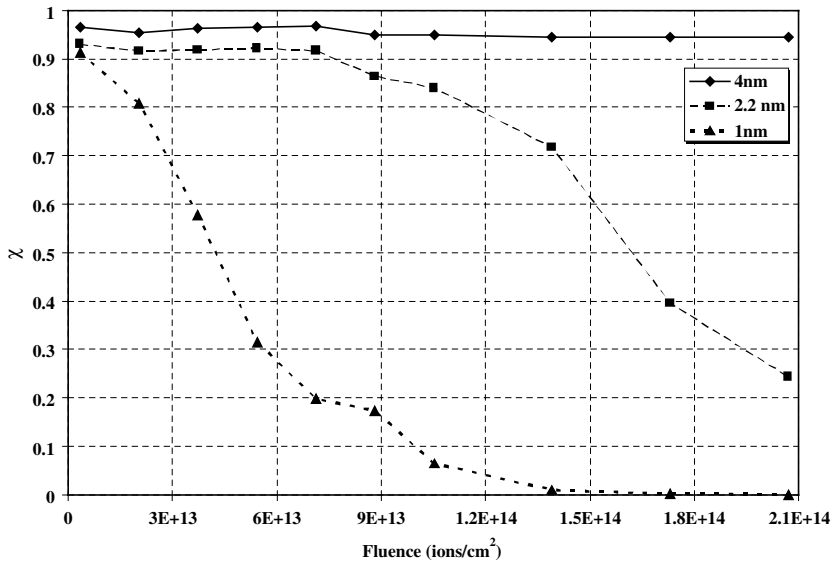

Fig. 8. Variation of crystallinity with respect to ion fluence (500 eV case). Data presented here are averaged over 8 separate randomized cases each with fluences up to more than 2×10^{14} ions/cm^2.

similar plateaus in the time evolution of potential energy per atom due to interaction of interstitial–vacancy pairs are reported by Marqués et al. in [29], there is no direct evidence that this is the case here. While Figs. 6 and 7 show results for individual representative 500 and 700 eV cases, Figs. 8 and 9 show crystallinity plots over an average of 8 and 5 cases of 500 and 700 eV ions, respectively.

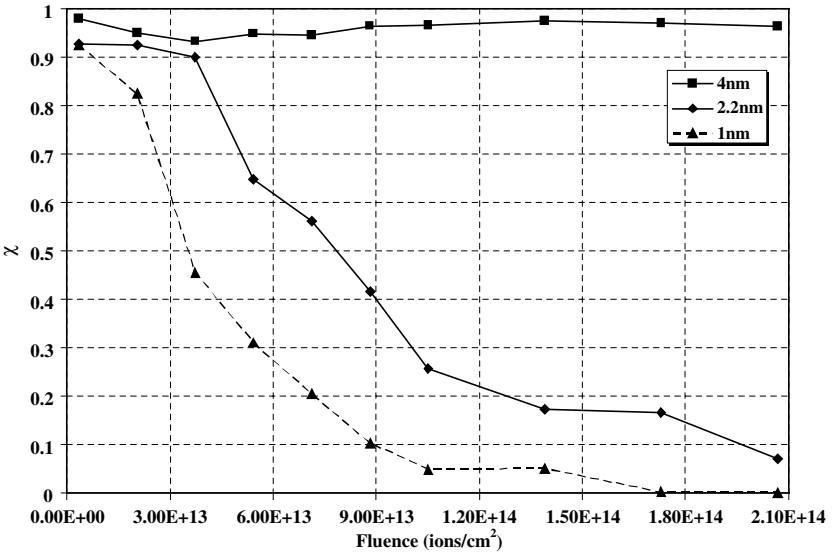

Fig. 9. Variation of crystallinity with respect to ion fluence (700 eV case). Data presented here are averaged over 5 separate cases.

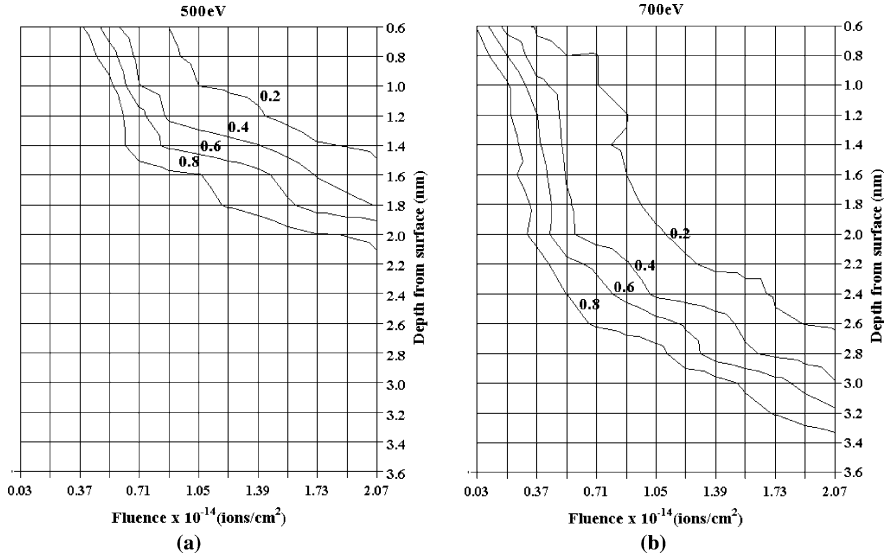

Fig. 10. Contour plot of variation of crystallinity with respect to ion fluence. Data presented here are averaged over 8 and 5 separate cases for 500 and 700 eV ion energies, respectively.

The plateau region is mostly obscured when the data are averaged over multiple cases. Fig. 10 shows a contour plot of variation of crystallinity, averaged over 5 cases of 700 eV ions. The difference between Fig. 10(a) and (b) illustrates the relative flatness of the amorphous/crystalline interface region of the 500 eV case compared to the 700 eV case.

3.1.4. Surface structure

The surface of crystalline silicon roughens under ion bombardment. The process of surface roughening is illustrated in Fig. 11 where color indicates the height of the atoms with red being above the original surface and dark blue indicating a depth of 1 nm below the original surface. The first image (a) shows the surface after just one impact, which leaves a small depression in the surface. The second figure (b) shows the configuration after 10 ions have impacted the surface. There is still some local order remaining near the upper-right and lower-left edges. The surface completely roughens over the next 10 ions and continues to change with additional ion impacts. An example of the fully roughened surface is given in (c) showing the surface after 50 ion impacts. The green areas indicate valleys and red indicates positions above the original surface height. This process is evidence of the incipient surface instability that leads to rippling and nanostructure formation in ion bombarded silicon. As the initial roughness forms, the well-known local angle dependence of the sputter yield renders the surface unstable.

3.2. Sputtering

Upon bombardment by argon ions, near-surface silicon atoms receiving sufficient energy are sputtered. Sputtering and implantation data are shown in Fig. 12 for fluences up to 4.0×10^{14} ions/cm^2 for individual cases of 500 and 700 eV each. The bursts that appear in individual cases (for example, at ion 80 in Fig. 12) are smoothed out when the data is averaged over randomized cases. Approximately one argon ion is implanted into the silicon for each argon ion incident on the surface for the 700 eV case. The rate of implantation for the 700 eV case is slightly higher than that of the 500 eV case, in which roughly 4 out of every 5 incident argon ions are successfully implanted. In the 500 eV case the silicon is sputtered away at a rate of ~1 silicon atom for every 2 argon ions inserted. The sputtering rate is slightly higher for the 700 eV case as would be expected since more energy is deposited into the system. The data shown in Fig. 12 demonstrate the observation that at higher fluences there is much more variability in sputter behavior. For example, for fluences of more than 2.5×10^{14} ions/cm^2, there is a series of significant jumps in the sputtered silicon and implanted argon counts. These features are not seen at low fluences when the system is still predominantly uniform and crystalline. Thus, sputtering behavior can only be properly accounted for when the target material has reached a steady state damaged structure.

3.2.1. Average sputter yield

The sputter yield is defined as the average number of silicon atoms sputtered per argon ion inserted into the system. Fig. 13 shows the sputter yields for the averaged 500 and 700 eV cases. The 700 eV case shows an average yield of 0.67 while the 500 eV case shows an average yield of 0.49. Haddeman and Thijsse [11] compare the computed sputter yield for Stillinger–Weber silicon bombarded by argon ions to experimental data for a range of energies. For normal incidence at 500 eV they report a sputter yield of ~0.45 that decreases with increasing fluence, while the experimental

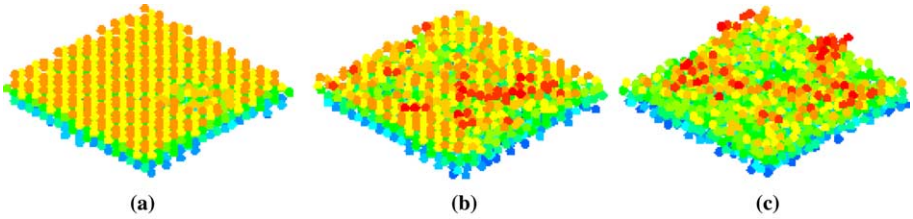

Fig. 11. The process of surface roughening. (a) Surface after 1 ion impact. (b) Surface after 10 ions impacts. (c) Sample of fully roughened surface. The colors indicate the height of the atoms, with red indicating a small distance above the original surface and dark blue indicating 1 nm below the original surface.

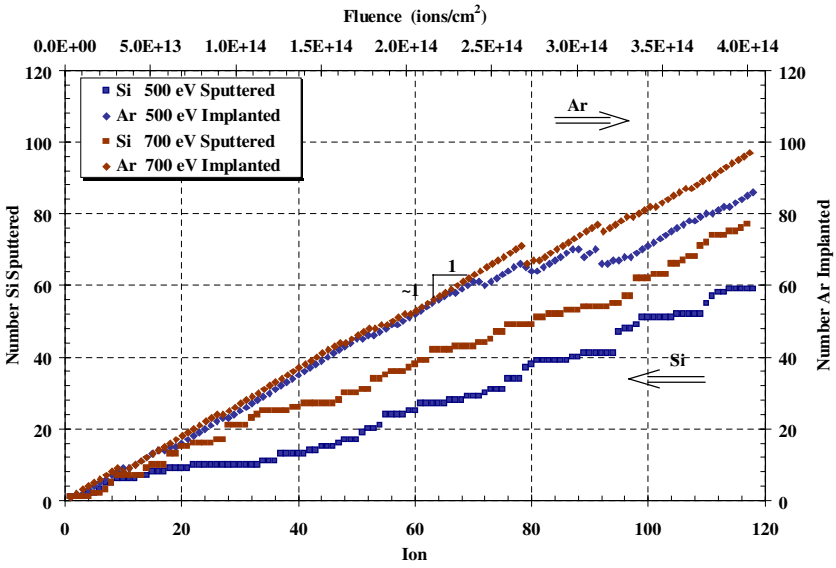

Fig. 12. Sputtering rates of silicon and argon for a case at each incident energy. There are significant jumps in the number of argon implanted and the number of silicon sputtered after fluences of 2.5×10^{14} ions/cm^2.

sputter yield [30] is constant at 0.68. The average sputter yield obtained from Fig. 13 exceeds the Haddeman and Thijsse [11] result by only 8%. However Haddeman and Thijsse consider fluences on the order of 10^{15} ions/cm^2 while the largest fluence considered in this study is approximately 5×10^{14} ions/cm^2. If the trend of decreasing sputter yield observed in [9] is obtained by the present approach for larger fluences the resulting sputter yields would be in better agreement. The difference between experimental sputter yields and simulated Stillinger–Weber values has been shown before [9].

It should also be noted that in both the 500 eV case and the 700 eV cases there is an initial transient trend toward higher instantaneous sputter yield, by as much as 20% in both cases. Discounting the first instantaneous sputter count, the instantaneous sputter yield increases monotonically until about 5×10^{13} ions/cm^2, approximately doubling, before decreasing to the steady state value.

3.2.2. Sputter bursts at high argon fluence

A typical ion impact does not sputter any silicon atoms. However, it is not uncommon for a single impact to sputter three or even more silicon atoms. Incident argon also typically sputters already-implanted argon in combinations of as many as three or more atoms at once. This observation is of interest because higher local concentration of argon might be expected to correlate with more significant individual sputtering events [15]. In this case the 700 eV argon energy case is considered since the sputtering rate is slightly higher than at 500 eV, and only one case is considered in order to retain features of the individual sequence of sputter events.

Fig. 14 shows a parametric plot in which both implanted argon and total sputter yield are dependent variables, while time (fluence) proceeds along the curve from left to right. Thus, bursts in sputtering are indicated by jumps up (due to bursts of silicon sputtering) or jumps *left* (due to loss of Argon at the surface). The vertical magnitude of the jumps in the plot generally decreases with increasing fluence, because the total sputter yield is less affected by individual events at larger total fluences. But there are several large burst events even at fluences of more than 2×10^{14} ions/cm^2. The number of implanted argon is affected by two large burst events that shift the curve left. The total sputter yield averages approximately 0.7–0.8,

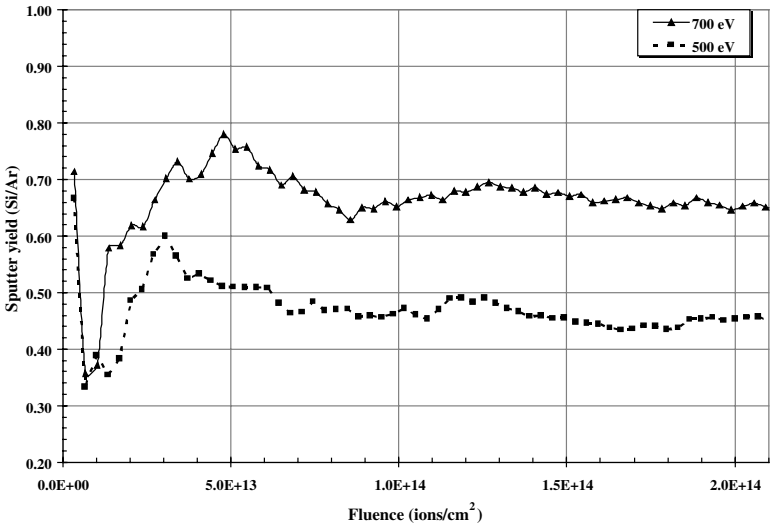

Fig. 13. Sputter yield as a function of fluence. Yield has been averaged over 8 separate randomized cases seeds for 500 eV incident ion energy and 5 separate randomized cases for 700 eV incident ion energy.

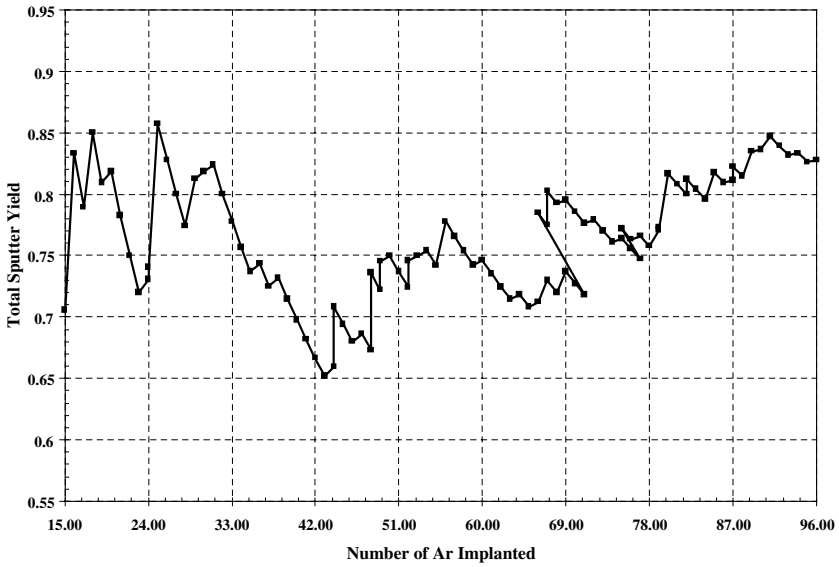

Fig. 14. Parametric plot of 700 eV sputtering, with both sputter yield and number of implanted argon as dependent variables. Time or total fluence proceeds from left to right. The end of the curve corresponds to 118 total impacts or a fluence of 4×10^{14} ions/cm^2.

and declines steadily between sputter burst events. This observation can be interpreted as a type of surface instability. Most implantation events take place without any resulting sputtering. Often three to five ions are implanted consecutively without any sputtering, during which time the surface evolves into a less stable structure as a result of accumulating damage that is not quite sufficient to sputter any atoms. Then a sputter burst occurs, resetting the surface in a more stable configuration

before the process is repeated. However, despite the evidence for this mechanism, the data show no apparent correlation between the number of atoms sputtered per ion and the number of argon atoms located under the impact. This contradicts the findings of Rubio et al. [15] who show an increase in the number of atoms sputtered per ion with an increase in fluence and also link increases in sputtering to the amount of argon beneath the impact area. However, Rubio et al. consider systems with 10% and 22% argon, whereas in this study there is only 2% argon present even at the largest fluence. Thus, it is concluded here that at low levels of fluence the argon content has no effect on sputtering but as fluence increases some individual impact events may sputter more atoms due to the larger local argon content. This process occurs by the sputter burst mechanism shown in Fig. 14, in which the increasingly unstable surface is periodically reset by bursts in the number of atoms sputtered away.

4. Conclusions

From a structural perspective, an initially clean (0 0 1) silicon surface roughens completely under ion bombardment after a total fluence of only approximately 1×10^{14} ions/cm^2. Damage within the bulk is characterized using a measure of crystallinity derived from a planar radial distribution function. By this measure, the region within about 1.5 nm of the free surface is essentially amorphous at fluences on the order of 1×10^{14} ions/cm^2. Only 3–4 nm below the surface, depending on the incident ion kinetic energy, the material is mostly defect free and crystalline, with small clusters of vacancy–interstitial complexes near the ends of the damage cascades.

Nearly all of the incident argon ions, modeled using a Molière type potential for interactions with silicon, are implanted. The argon ions not implanted significantly deeper than 1 nm are eventually annealed out at the free surface. In the 500 eV case, the implanted argon is nearly completely localized in the damaged or amorphous layer. In the 700 eV, significantly more argon ions penetrate into the crystalline material below.

Collisions with the argon lead to sputtering of the silicon. Sputter yields or rates are higher at 700 eV incident energy than at 500 eV incident energy. In both cases, there is an initial transient behavior that shows sputter yields up to 20% higher than the steady state values of 0.7 (atoms sputtered per impact) for the 700 eV case and 0.5 for the 500 eV case. As sputtering proceeds the average sputter yield remains steady. But at higher fluences, the sputtering proceeds in short bursts of up to three or more sputtered atoms; between these bursts the incident ions have little sputtering effect on the surface. Local implanted argon concentration is found to have little effect on the silicon sputtering behavior.

Acknowledgements

The support of NSF grant DMI 02-23821 is gratefully acknowledged. The authors also thank Prof. T.G. Bifano of Boston University for many helpful discussions.

References

[1] T.G. Bifano, H.T. Johnson, P. Bierden, R. Mali, J. MEMS 11 (2002) 592.
[2] L.A. Marqués, M.J. Caturla, H. Huang, T. Díaz de la Rubia, Mater. Res. Soc. Symp. Proc.: Ion–Solid Interactions for Materials Modifications and Processing 396 (1996) 201.
[3] D. Maric, L. Colombo, Mater. Res. Soc. Symp. Proc.: Crystallization and Related Phenomena in Amorphous Materials 321 (1994) 423.
[4] T. Díaz de la Rubia, G.H. Gilmer, Phys. Rev. Lett. 74 (1995) 2507.
[5] R. Smith, D.E. Harrison Jr., B.J. Garrison, Phys. Rev. B 40 (1989) 93.
[6] M.E. Barone, D.B. Graves, Plasma Sources Sci. Technol. 5 (1996) 187.
[7] A.M. Mazzone, Nucl. Instr. and Meth. B 183 (2001) 251.
[8] L.A Marqués, M.J. Caturla, T. Díaz de la Rubia, J. Appl. Phys. 80 (1996) 6160.
[9] N.A Kubota, D.J. Economou, S.J. Plimpton, J. Appl. Phys. 83 (1998) 4055.
[10] N.A. Kubota, D.J. Ecnonomou, IEEE Trans. Plasma Sci. 27 (1999) 1416.
[11] E.F.C. Haddeman, B.J. Thijsse, Nucl. Instr. and Meth. B 202 (2003) 161.

[12] M. Koster, H.M. Urbassek, Nucl. Instr. and Meth. B 180 (2001) 299.
[13] M. Kitabatake, J.E. Greene, Thin Solid Films 272 (1996) 271.
[14] S. Chiba, T. Aoki, J. Matsuo, Nucl. Instr. and Meth. B 180 (2001) 317.
[15] J.E. Rubio, L.A. Marqués, L. Pelaz, M. Jaraíz, J. Barbolla, Nucl. Instr. and Meth. B 112 (1996) 156.
[16] M.J. Caturla, T. Díaz de la Rubia, L.A. Marqués, Phys. Rev. B 54 (1996) 16683.
[17] T. Motooka, Mater. Sci. Eng. A 253 (1998) 42.
[18] B. Weber, K. Gärtner, D.M. Stock, Nucl. Instr. and Meth. B 127–128 (1997) 239.
[19] K. Gärtner, B. Weber, Nucl. Instr. and Meth. B 180 (2001) 274.
[20] J. Nord, K. Nordlund, J. Keinonen, Phys. Rev. B 65 (2002) 165329.
[21] P. Partyka, Y. Zhong, K. Nordlund, R.S. Averback, I.M. Robinson, P. Ehrhart, Phys. Rev. B 64 (2001) 235207.
[22] F. Stillinger, T. Weber, Phys. Rev. B 31 (1985) 5262.
[23] V.G. Molière, Z. Naturforschg. 2a (1947) 133.
[24] I.M. Torrens, Interatomic Potentials, Academic Press, New York, 1972.
[25] A. Delcorte, B.J. Garrison, J. Phys. Chem. B 104 (2000) 6785.
[26] H. Berendsen, J. Postma, F. van Gunsteren, A. DiNola, J. Haak, J. Chem. Phys. 81 (1984) 3684.
[27] M.P. Allen, D.T. Tildesley, Computer Simulations of Liquids, Clarendon Press, Oxford, 1987.
[28] D.L. Williamson, S. Roorda, M. Chicoine, R. Tabti, P.A. Stolk, S. Acco, F.W. Saris, Appl. Phys. Lett. 67 (1995) 226.
[29] L.A. Marqués, L. Pelaz, J. Hernandez, J. Barbolla, Phys. Rev. B 64 (2001) 45214.
[30] P.C. Zalm, J. Appl. Phys. 4 (1983) 2662.